THE JOURNAL OF CHEMICAL PHYSICS **135**, 024509 (2011)

Dynamics of self-propelled nanomotors in chemically active media

Snigdha Thakur[a] and Raymond Kapral[a]
Chemical Physics Theory Group, Department of Chemistry, University of Toronto,
Toronto, Ontario M5S 3H6, Canada

(Received 11 April 2011; accepted 13 June 2011; published online 13 July 2011)

Synthetic chemically powered nanomotors often rely on the environment for their fuel supply. The propulsion properties of such motors can be altered if the environment in which they move is chemically active. The dynamical properties of sphere dimer motors, composed of linked catalytic and noncatalytic monomers, are investigated in active media. Chemical reactions occur at the catalytic monomer and the reactant or product of this reaction is involved in cubic autocatalytic or linear reactions that take place in the bulk phase environment. For these reactions, as the bulk phase reaction rates increase, the motor propulsion velocity decreases. For the cubic autocatalytic reaction, this net effect arises from a competition between a reduction of the nonequilibrium concentration gradient that leads to smaller velocity and the generation of fuel in the environment that tends to increase the motor propulsion. The role played by detailed balance in determining the form of the concentration gradient in the motor vicinity in the active medium is studied. Simulations are carried out using reactive multiparticle collision dynamics and compared with theoretical models to obtain further insight into sphere dimer dynamics in active media. © *2011 American Institute of Physics*. [doi:10.1063/1.3607408]

I. INTRODUCTION

Molecular motors that use chemical energy for their propulsion perform a variety of tasks that are essential for biochemistry in the cell.[1,2] These motors are able to operate in the presence of strong fluctuations and move from one place to another in the cell by directed motion that is more effective than simple diffusion. Synthetic chemically powered motors, which have similar sizes and move with comparable velocities to those of biological motors, have been fabricated. Such synthetic motors are of interest since they have the potential to be used in applications that benefit from active transport instead of normal diffusion.

Various types of synthetic motors have been constructed. Perhaps the most studied self-propelled objects of this kind are metallic nano and micron scale rod-shaped motors.[3–7] In Pt-Au rod motors catalytic decomposition of hydrogen peroxide or other fuel occurs at the Pt end and the propulsion mechanism is electrochemical in nature.[8,9] Striped metallic rod motors, where Ni is incorporated to allow the motor to be guided by external magnetic fields, have been made and used to show that targetted cargo delivery can be achieved.[10–12] Motors with high velocities have been made from carbon-nanotube-supported metallic rods with hydrazine as fuel.[9] Carbon fibers have been autonomously propelled through an electrochemical mechanism by the enzyme catalyzed glucose-oxygen reaction.[13] A number of other applications have been demonstrated and these studies have served to indicate the potential utility of synthetic motors.[14]

In addition to metallic rod motors, sphere dimer[15] and Janus particle[16] silica-Pt motors, which also use hydrogen peroxide as fuel but operated by different mechanisms, have been fabricated and their dynamics has been investigated. Mesoscopic models have been constructed and used to simulate the sphere dimer dynamics and elucidate the nature of the propulsion mechanisms.[15,17–19] Colloidal Janus particles that exhibit directed motion have also been studied theoretically and experimentally.[20–25]

Most synthetic chemically powered motors have the common feature that they do not carry their fuel; instead it is supplied by the surrounding medium in which they move. If the medium in which the motor moves is itself chemically active, this can influence the motor dynamics. For example, the reaction products can be consumed in environmental reactions and thereby change the nonequilibrium concentration gradients that are a central element of the propulsion mechanism. One can consider more complex reaction kinetics in the medium and such kinetics may influence the motor dynamics in more subtle ways.

In this article, we investigate the dynamics of a chemically powered sphere dimer motor, which consists of linked catalytic and noncatalytic spheres, in a chemically active medium. In Sec. II we describe the reactive mesoscopic method used to simulate the motor dynamics and also discuss how the propulsion velocity can be estimated from a knowledge of the intermolecular forces and the nonequilibrium concentration fields in the system. The discussion is presented in general terms that allow for arbitrary reactions at the catalytic sphere and arbitrary reactions in the bulk phase. Section III considers two specific examples of chemically active media: a cubic autocatalytic reaction and a linear reaction in which the reaction product from dimer catalytic reaction is consumed. This section presents the simulation results and discusses the role played by detailed balance in the motor

---

[a] Electronic addresses: sthakur@chem.utoronto.ca and rkapral@chem.utoronto.ca.

dynamics when the cubic autocatalytic reaction occurs in the bulk phase. Theoretical models for the phenomena are presented in Sec. IV and compared to the simulation results. Section V describes the translational diffusion and orientational relaxation times for the self-propelled sphere dimers. The conclusions are given in Sec. VI.

II. NANOMOTOR AND ITS ENVIRONMENT

Chemically powered sphere dimer motors consist of linked catalytic (C) and noncatalytic (N) spherical monomers. The directed motion of a dimer motor is due to a propulsion force F_{prop} that arises from the interactions of the dimer monomers with the chemical species X_α in its environment, and the chemical reaction that occurs with rate $\mathcal{R}_\alpha^c$ on the surface of the catalytic monomer.[17–19] We consider the general case where the environment in which the motor moves is itself chemically active. We assume that various chemical reactions,

$$\sum_\alpha \nu_\alpha^j X_\alpha \underset{k_{-j}}{\overset{k_j}{\rightleftharpoons}} \sum_\alpha \bar{\nu}_\alpha^j X_\alpha \quad (j = 1, \ldots, r)\,, \tag{1}$$

labeled by the index j, occur in the medium. In this equation ν_α^j and $\bar{\nu}_\alpha^j$ are the stoichiometric coefficients for reaction j and k_j and k_{-j} are the rate constants that characterize the forward and reverse reactions. Nanomotors are subject to strong fluctuations from the environment and our simulations of sphere dimer motors in active media utilize a particle-based mesoscopic molecular dynamics method for the evolution that can account for such fluctuations.[26,27] From these simulations we can compute the forces on the nanomotor and determine its velocity and other properties. However, in order to gain insight into the factors that determine the motor velocity, it is useful to consider approximate theoretical expressions that can be used to estimate this quantity. Below we describe both the mesoscopic simulation method for the motor dynamics in an active medium and the theoretical estimate for the motor velocity.

A. Mesoscopic simulation method

The dynamics in the reactive environment is simulated using reactive multiparticle collision (RMPC) dynamics.[28–30] RMPC dynamics consists of a concatenation of multiparticle collisions that change the velocities of the particles and birth-death stochastic reactive events. Nonreactive events occur by multiparticle collision (MPC) dynamics. The implementation of MPC dynamics and examples of its applications are described in reviews[31,32] and references therein. Briefly, to carry out multiparticle collisions, at time intervals τ the point-like solvent molecules are sorted into cubic cells with linear dimension a_0 and rotation operators $\hat{\omega}_\xi$ are assigned to each cell from some set of rotation operators. Multiparticle collisions are performed independently in each cell, and in these collisions the postcollision velocity of particle i in cell ξ is given by $\mathbf{v}_i' = \mathbf{V}_\xi + \hat{\omega}_\xi(\mathbf{v}_i - \mathbf{V}_\xi)$, where $\mathbf{V}_\xi$ is the center-of-mass velocity of the particles in that cell.

Reactive multiparticle collisions combine such velocity-changing events with a birth-death stochastic description of reactions. Specifically, a reaction,

$$\sum_\alpha \nu_\alpha^j X_\alpha \xrightarrow{k_j} \sum_\alpha \bar{\nu}_\alpha^j X_\alpha, \tag{2}$$

is assumed to occur with probability

$$p_j^\xi(\mathbf{N}^\xi) = \frac{a_j^\xi}{a_0^\xi}(1 - e^{-a_0^\xi \tau}), \tag{3}$$

where $\mathbf{N}^\xi = (N_1^\xi, N_2^\xi, \ldots,)$ is the set of numbers of the different species in cell ξ. Here

$$a_j^\xi = k_j(V_c) \prod_\alpha \frac{N_\alpha^\xi!}{\left(N_\alpha^\xi - \nu_\alpha^j\right)!}, \tag{4}$$

where the notation $k_j(V_c)$ indicates that the rate constants have been scaled for the cell volume V_c. The combinatorial factor accounts for the number of different ways the reaction can occur in the cell. The quantity a_0^ξ is given by $a_0^\xi = \sum_j a_j^\xi$. The combination of reactions and multiparticle collisions models coarse grained reactive and non-reactive collisions in the system.

The monomers of the sphere dimer interact with the particles in the environment through intermolecular potentials and in the time intervals τ between multiparticle collisions the evolution is described by molecular dynamics (MD). Since there are no solvent-solvent forces to compute in the MD segments, the simulations are easily carried out, even in systems with a large number of environmental particles. In summary, in the hybrid MD-RMPC dynamics used to study the sphere dimer motion, at time intervals τ the system is divided into collision cells and reactive multiparticle collisions are carried out independently in each cell. The system, dimer and solvent molecules, is then propagated for a time τ by Newton's equations of motion after which the next RMPC collision events take place. The reactive dynamics conserves mass, momentum and energy and thus accounts for hydrodynamic and solvent diffusion effects on the dimer dynamics.

B. Estimate of motor velocity

Micron and nanoscale chemically powered motors move with small velocities in a viscous medium and, since viscous forces dominate inertial forces, their Reynolds numbers are small. In this case we can neglect inertial terms and, considering the average motion in the steady state, the propulsion force is balanced by the frictional force, $F_{\text{prop}} + F_{\text{fric}} = 0$. Here $F_{\text{fric}} = -\zeta V_z$ with ζ the friction coefficient. The motor velocity is then given by $V_z = F_{\text{prop}}/\zeta$. To compute V_z, we require an expression for the steady state propulsion force, which depends on the nonequilibrium species concentration fields $\rho_\alpha(\mathbf{r})$ that arise from the chemical reactions at the C monomer. The propulsion force can be written explicitly as[17]

$$F_{\text{prop}} = -\sum_\alpha \int d\mathbf{r}\,\rho_\alpha(\mathbf{r}) \frac{dV_{C\alpha}(r)}{dr}(\hat{\mathbf{z}} \cdot \hat{\mathbf{r}}) - \sum_\alpha \int d\mathbf{r}'\,\rho_\alpha(\mathbf{r}' + R\hat{\mathbf{z}}) \frac{dV_{N\alpha}(r')}{dr'}(\hat{\mathbf{z}} \cdot \hat{\mathbf{r}}'), \tag{5}$$

where the vector distance from the center of C to a solvent molecule is $\mathbf{r}$, while $\mathbf{r}' = \mathbf{r} - R\hat{\mathbf{z}}$ has origin at N, where R the bond length of the dimer and $\hat{\mathbf{z}}$ is a unit vector from N to C. Since the intermolecular forces are known in our mesoscopic model, the main difficulty in the computation of F_{prop} is the specification of the spatial dependence of $\rho_\alpha(\mathbf{r})$. To estimate this quantity we adopt a macroscopic description outside of a boundary region around the monomers of the sphere dimer and write

$$\rho_\alpha(\mathbf{r}) = n_\alpha(\mathbf{r}) e^{-\beta[V_{C\alpha}(r) + V_{N\alpha}(r')]}, \tag{6}$$

where the Boltzmann factor accounts for the exclusion of A and B particles from the monomers as a result of the solvent-monomer intermolecular forces and $n_\alpha(\mathbf{r})$ may be found from the solution of a reaction-diffusion equation in the bulk phase environment. Given that reactions (1) occur in the environment, the net rate of reaction for species X_α, $\mathcal{R}_\alpha(\mathbf{n})$, follows from mass action kinetics and is given by

$$\mathcal{R}_\alpha(\mathbf{n}) = \sum_j (\bar{\nu}_\alpha^j - \nu_\alpha^j) \left[k_j \prod_\beta n_\beta^{\nu_\beta^j} - k_{-j} \prod_\beta n_\beta^{\bar{\nu}_\beta^j} \right], \tag{7}$$

where $\mathbf{n} = \{n_\alpha\}$, with n_α the number density of species X_α. Consequently, the reaction-diffusion equation may be written as

$$\frac{\partial n_\alpha(\mathbf{r}, t)}{\partial t} = D_\alpha \nabla^2 n_\alpha(\mathbf{r}, t) + \mathcal{R}_\alpha(\mathbf{n}(\mathbf{r}, t)), \tag{8}$$

where D_α is the diffusion coefficient of species X_α. This reaction-diffusion equation must be solved in the steady state subject to boundary conditions at the dimer surface and at infinity. As $r \to \infty$ we assume that the concentration fields are either fixed by fluxes into and out of the system to maintain a steady state, or by the nonequilibrium state of the reactive medium far from the dimer. At the catalytic monomer surface R_0 we apply a "radiation" boundary condition[33] to account for the reaction that occurs there,

$$\mathcal{R}_\alpha^c(\mathbf{n}(R_0)) + 4\pi D_\alpha R_0^2 \frac{d}{dr} n_\alpha(r)\Big|_{R_0} = 0, \tag{9}$$

while at the noncatalytic sphere a reflection boundary condition may be used, whose form is similar to that in Eq. (9) with the reaction term set to zero.

The nonequilibrium steady state concentration fields obtained in this way may be substituted into Eq. (5) to give the propulsion force. The friction coefficient of the dimer can be estimated either from kinetic theory and Stokes law or obtained from the simulation to complete the calculation of the sphere dimer velocity.

III. PROPULSION IN AN ACTIVE MEDIUM

In the simulations of sphere dimer motion described in this section, the reaction,

$$A + C \underset{k_{-1}}{\overset{k_1}{\rightleftharpoons}} B + C, \tag{10}$$

is assumed to occur at the catalytic monomer with rate $\mathcal{R}_A^c(\mathbf{n}(R_0)) = -k_1^0 n_A(R_0) + k_{-1}^0 n_B(R_0)$, where k_1^0 and k_{-1}^0 are intrinsic reaction rate constants that characterize the forward and reverse reactions in the boundary layer around the catalytic monomer. In our simulations the reaction $A \to B$ occurs with probability p_+ whenever A encounters C. The reverse reaction occurs with probability $p_- = 1 - p_+$ on encounter of B with the C monomer, although the forward and reverse reaction probabilities could have been chosen independently.[18] The irreversible reaction $A \to B$ corresponds to $p_+ = 1$. These probabilities, along with the collision frequencies of the A and B species with the catalytic sphere, determine the $k_{\pm 1}^0$ intrinsic rate constants. Since the A and B molecules must encounter the C sphere before reaction can take place, there is also a diffusion-controlled component that contributes to the full $k_{\pm 1}$ rate constants for the C catalytic reaction in the system. We shall describe below how these rate coefficients can be determined from the simulations and theoretically estimated.

We also suppose that the cubic autocatalytic chemical reactions,

$$B + 2A \underset{k_{-2}}{\overset{k_2}{\rightleftharpoons}} 3A, \tag{11}$$

occur in the environment with rate,

$$\mathcal{R}_A = -\mathcal{R}_B = k_2 n_B(\mathbf{r}, t) n_A^2(\mathbf{r}, t) - k_{-2} n_A^3(\mathbf{r}, t). \tag{12}$$

In the RMPC simulations, for the cubic autocatalytic reaction, the quantities a_j^ξ have the forms $a_2^\xi = k_2 N_B^\xi N_A^\xi (N_A^\xi - 1)$ and $a_{-2}^\xi = k_{-2} N_A^\xi (N_A^\xi - 1)(N_A^\xi - 2)$ for the forward and reverse reactions in Eq. (11), respectively.[29] While special, this is an interesting set of bulk phase reactions to consider since the B species which is produced from A in the forward reaction at the catalytic monomer is converted back to A in the environment.[56] This has consequences for the nature of the nonequilibrium steady state that is established in the system and role that detailed balance plays in propulsion.

For comparison, we also consider the simpler situation where the B species is simply converted another species D by the reaction,

$$B \overset{k_3}{\to} D, \tag{13}$$

that occurs with rate $\mathcal{R}_B = -k_3 n_B$. The corresponding a_j^ξ quantity for the RMPC simulations is $a_3^\xi = k_3 N_B^\xi$. The species D is not involved in the catalytic reaction at C.

A. Simulation parameters

In our simulations the bulk phase species have identical masses and interact with the sphere dimer monomers through repulsive 6-12 Lennard-Jones (LJ) potentials, $V_{S\alpha}(r) = 4\epsilon[(\sigma_S/r)^{12} - (\sigma_S/r)^6 + 1/4]$, $r \le r_c$, with cutoff distance $r_c = 2^{1/6}\sigma_S$. We use the notation $V_{S\alpha}$, where $S = C, N$ and $\alpha = A, B$ to denote the various interaction potentials between solvent and dimer monomers.[17–19] We take $V_{AC} = V_{BC} = V_{AN}$, which are characterized by the energy and distance parameters ϵ_A and σ_S, respectively; however, interactions between the N sphere and B molecules, V_{BN}, have energy parameter ϵ_B.

In our simulations, all quantities are reported in dimensionless units based on energy ϵ_A, mass m_A, and distance σ_A parameters. We chose the average number of particles per cell to be $n_0 \approx 9$ in all simulations. The rotation operators for MPC dynamics are taken to correspond to rotations about a randomly chosen axis by an angle of $\pi/2$. In the dimensionless units the MPC cell size is $a_0 = 1$. The masses of both A and B species are taken to be $m = 1$. The masses of the catalytic and noncatalytic spheres are adjusted according to their diameters, d_C and d_N, to ensure that the mass densities of the monomers are approximately same as those of the solvent. The MD time step used to integrate Newton's equation of motion with the velocity Verlet algorithm is $\Delta t = 0.01$, while the multiparticle collision time is $\tau = 0.5$. The system is contained in a cubic box of volume V and linear dimension $L = 40$ with periodic boundary conditions. The system temperature is $k_B T = 0.2$ and the LJ potential parameters are chosen to be $\epsilon_A = 1.0$ and $\epsilon_B = 0.1$. The diameters of the catalytic and noncatalytic spheres are $d_C = 4.0$ and $d_N = 8.0$, respectively. The sphere dimer internuclear separation is fixed at $R = 7.0$ by a holonomic constraint.[34,35] This value of R insures that there are no discontinuous potential changes when chemical reaction occurs on the catalytic sphere. We also prevent discontinuous potential changes due to the bulk reactions by carrying out these reactions only outside the potential cutoff distance of the noncatalytic sphere. The reaction probability at the catalytic sphere and the reaction rate constants of the bulk phase reactions are varied in the simulations described below. For the parameters specified above the diffusion coefficients of solvent species are the same and denoted by D. Analytical expressions for D are available for MPC dynamics.[31,32] In order to insure that Galilean invariance is satisfied for systems with small mean free path λ, a random shift of the grid that defines the collision cells is carried out before the collision step.[36,37]

B. Simulation results

The velocity of the sphere dimer depends on the rates at which the reactions in the bulk phase occur, since these rates influence the local species concentration fields in the vicinity of the motor. First, we discuss the simple case where both the catalytic reaction at C and the bulk reaction are irreversible; i.e., the rate coefficients $k_{-1} = k_{-2} = 0$. Under such nonequilibrium conditions we see that the "fuel" A for the self propulsion, which is consumed at the C sphere, is regenerated in the bulk phase by the cubic autocatalytic reaction. No explicit fluxes of species at the boundary need to be introduced in the simulation to maintain the system in a steady state where the sphere dimer moves with average constant velocity. Of course, in a complete specification of the reactive dynamics one would have to account for the way the bulk reaction is maintained out of equilibrium. For example, the effective cubic autocatalysis could result from a sequence of elementary steps where fast intermediate species are eliminated from the rate equations and the system is subject to flows to maintain a nonequilibrium state.[38] Such effective rate processes are easily modeled in our coarse grained probabilistic description of the bulk phase reaction kinetics since RMPC reactive events are carried out at the MPC cell level at time intervals τ where many chemical species reside in a cell and many elementary events could have taken place in the time τ.

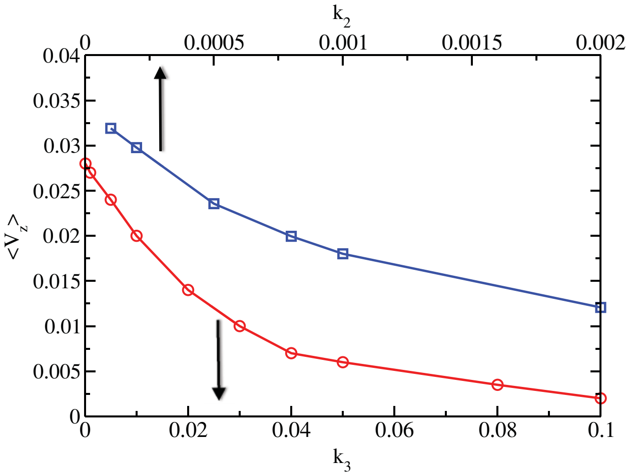

FIG. 1. The average velocity of the sphere dimer motor along its internuclear axis, $\langle V_z \rangle$, as a function of the rate constant k_2 for the irreversible cubic autocatalytic reaction and as a function of k_3 for the linear reaction. The velocity $\langle V_z \rangle$ for each value of k_2 and k_3 was determined from an average over ten independent realizations of the dynamics.

Figure 1 shows the steady state propulsion velocity of the dimer as a function of k_2. The simulation results were obtained by fitting the motor velocity probability distribution function $p(V_z)$ to a Maxwell-Boltzmann distribution from which the average velocity was determined. The dimer velocity decreases as the rate of the bulk phase reaction increases. This decrease can be attributed to the fact that the spatial decay of the B particle concentration field with increasing distance from the C sphere becomes more rapid as k_2 increases. The bulk autocatalytic reaction has both positive and negative effects on the sphere dimer propulsion. As noted above, it generates the fuel A that leads to the production of B, whose gradient at the N sphere is essential for propulsion; however, the $B + 2A \to 3A$ reaction will remove B particles in the bulk phase and reduce the B concentration gradient. The decrease in the sphere dimer velocity with increasing k_2 is due to the fact that at higher k_2 the bulk conversion B to A is sufficiently rapid to reduce the B field gradient at N. These observations are confirmed by the dependence of $n_B(r)$ on k_2 plotted in Fig. 2(a). One sees that $n_B(r)$ does indeed decay more rapidly as k_2 increases.

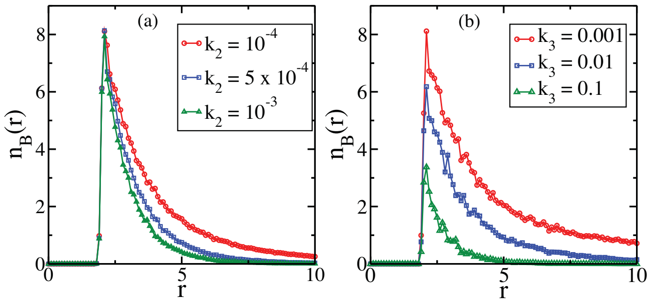

FIG. 2. (a) Plot of the B steady state density field $n_B(r)$ in the vicinity of the catalytic sphere C for different values of k_2 for irreversible reactions at the catalytic sphere and in the bulk phase. (b) The steady state concentration field of B particles for different values of rate constant k_3 for the linear bulk phase reaction.

A simple linear reaction $B \to D$ in the bulk phase that destroys B molecules has a similar effect on $n_B(r)$. Figure 2(b) is a plot of $n_B(r)$ where it is seen that the B field decays more rapidly as k_3 increases. The effect of this reaction on the dimer velocity is also shown in Fig. 1 as a function of k_3. Since this bulk phase reaction does not regenerate the fuel A, we must supply A at the boundaries to maintain a steady state; thus, when B or D molecules leave the simulation box, new A particles are introduced so that the A field far from the sphere dimer is specified.

C. Role of detailed balance

The detailed balance condition follows from the principle of microscopic reversibility and reflects the fact that the underlying equations of motion are time reversible; hence, at equilibrium each forward transition is as likely as the reverse transition.[39] In order to investigate the role that detailed balance plays in the propulsion of the sphere dimer, we now consider the reversible reaction case. At equilibrium the time variations of the concentrations described by mass action rate laws corresponding to Eqs. (10) and (11) are individually equal to zero: $-k_1 n_A^{\mathrm{eq}} + k_{-1} n_B^{\mathrm{eq}} = 0$ and $k_2 n_B^{\mathrm{eq}} (n_A^{\mathrm{eq}})^2 - k_{-2} (n_A^{\mathrm{eq}})^3 = 0$. It then follows that detailed balance places restrictions on the allowed values of the rate constants for this set of reactions and we have

$$\frac{k_1}{k_{-1}} = \frac{k_{-2}}{k_2} = \frac{n_B^{\mathrm{eq}}}{n_A^{\mathrm{eq}}}. \tag{14}$$

We investigated the sphere dimer propulsion for three different cases: (i) when both the C catalytic reaction and the bulk autocatalytic reaction are irreversible, (ii) when the reactions are reversible, but the reaction rates do not satisfy detailed balance, and (iii) when the reactions are reversible and the reaction rates obey the detailed balance condition. The reaction rate coefficients and reaction probabilities for above cases are: (i) $p_+ = 1.0$, $p_- = 0.0$, $k_2 = 10^{-4}$, $k_{-2} = 0.0$; (ii) $p_+ = 0.8$, $p_- = 0.2$, $k_2 = 10^{-4}$, $k_{-2} = 10^{-5}$; and (iii) $p_+ = 0.5$, $p_- = 0.5$, $k_2 = 10^{-4}$, $k_{-2} = 10^{-4}$ (the relation between $p_\pm$ and $k_{\pm 1}$ is given below). The velocity probability distribution functions $p(V_z)$ of the dimer are shown in Fig. 3 for these three cases. The average velocities of the dimer in cases (i)-(iii), determined from the simulation data, are $V_z = 0.034$, 0.022, and 0.0, respectively. As expected, the sphere dimer does not exhibit directed motion when the reactions obey detailed balance, reinforcing the fact that dimer propulsion is a nonequilibrium effect.

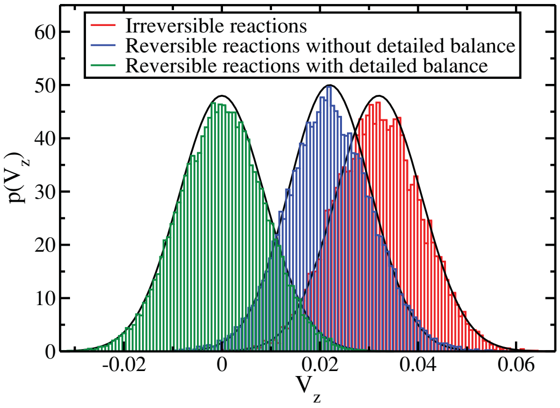

FIG. 3. Probability distribution function $p(V_z)$ of the center-of-mass velocity of the dimer projected along the internuclear axis for an irreversible reaction (i), a reversible reaction violating detailed balance (ii), and a reversible reaction satisfying detailed balance (iii).

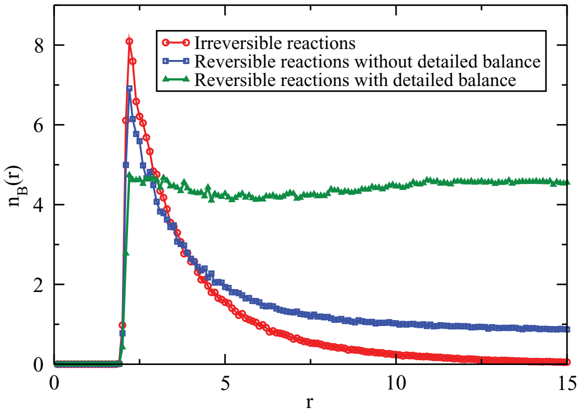

FIG. 4. The local steady state concentration of B particles around the catalytic sphere C for an irreversible reaction, a reversible reaction which breaks the detailed balance, and a reversible reaction which satisfies detailed balance. The reaction rates for these cases are given in the text.

These dimer propulsion results can be understood in terms of the local steady state concentration of species B in the vicinity of the catalytic C sphere shown in Fig. 4. The existence of a strong B concentration gradient for the irreversible reaction is evident, which then gives rise to a high propulsion velocity. For a reversible reaction satisfying detailed balance, there is no nonequilibrium B concentration gradient around the dimer; hence, directed dimer propulsion cannot occur. (The small deviation from a flat concentration profile is due to the presence of the noncatalytic N sphere.) If reversible reactions are considered but detailed balance is broken, again a considerable nonequilibrium B concentration gradient exists in the vicinity of the dimer motor. The nature of the B particle concentration gradient can be understood in terms of the magnitudes of the reaction rate constants. In cases (i) and (ii) the rate constants are such that the number of B particles produced by the bimolecular catalytic reaction at C is much greater than the number converted back to A by the bulk phase cubic autocatalytic reaction. However, in case (iii) where detailed balance is satisfied, the rate coefficients obey Eq. (14); hence, the B particles produced by the C catalytic reaction are converted back to A at the same rate, yielding a flat B concentration profile. These observations confirm the necessity to break detailed balance for self-propulsion.[40]

IV. THEORETICAL DESCRIPTION

In Sec. II we described how the sphere dimer propulsion velocity could be estimated. The estimate requires the calculation of the propulsion force from Eq. (5). This calculation, in turn, requires a knowledge of the nonequilibrium steady state concentration fields, which may be estimated from the

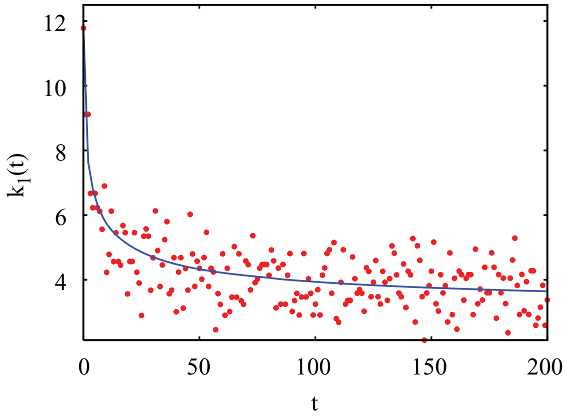

FIG. 5. Plot of the time dependent rate coefficient $k_1(t)$ versus time (points). The solid line is a fit to the data using Eq. (15).

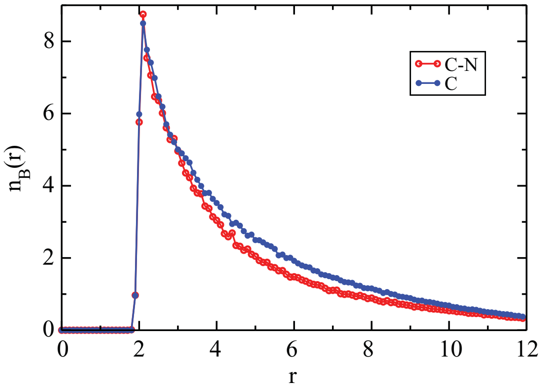

FIG. 6. Plot of $n_B(r)$ versus r showing the effect of the presence of the noncatalytic sphere N on the B density field. Results are for the case when there no bulk phase reaction in the system.

solution to the reaction-diffusion Eq. (8) in the steady state, subject to the boundary conditions in Eq. (9). Both the reaction-diffusion equation and its boundary conditions require the rate constants and diffusion coefficients as input. The bulk phase rate constants are directly specified in the RMPC stochastic model. As noted earlier, while the reaction probabilities at the C sphere and the collision frequency determine the intrinsic $k^0_{\pm 1}$ rate constants, there is also a diffusion-influenced component that may control the rate. In addition to these quantities that enter in the propulsion force, the friction coefficient of the sphere dimer is needed to complete the calculation of the velocity. In this section we describe how these quantities may be estimated and compare the estimates with simulation results. We then use these quantities to calculate the propulsion velocities for the sphere dimer in the chemically active media discussed above.

A. Parameter estimates

We first consider the value of the rate constant k_1. (A similar calculation can be carried out to obtain k_{-1}.) The simplest situation to consider is an irreversible reaction at a single catalytic C sphere, $A + C \to B + C$, occurring in a chemically inactive medium initially composed of A particles. The rate law for this case may be written as $dn_A(t)/dt = -k_1(t) n_C n_A(t)$, which defines $k_1(t)$, the time-dependent rate coefficient. The time-dependent rate coefficient obtained from the simulation[41] by computing $-[dn_A(t)/dt]/[n_A(t)n_C]$ is plotted in Fig. 5.

The rate coefficient $k_1(t)$ can be calculated by solving the diffusion equation, $\partial n_A(\mathbf{r}, t)/\partial t = D\nabla^2 n_A(\mathbf{r}, t)$, subject to the radiation boundary condition, $4\pi D R_0^2 (dn_A(r)/dr)\,|_{R_0} = k_1^0 n_A(R_0)$, applied at R_0, an effective C catalytic sphere radius outside of which the diffusion equation applies. The result is[42,43]

$$k_1(t) = \frac{k_1^0 k_D}{k_1^0 + k_D} + \frac{(k_1^0)^2}{k_1^0 + k_D} \exp\left[\left(1 + \frac{k_1^0}{k_D}\right)^2 \frac{Dt}{R_0^2}\right] \times \operatorname{erfc}\left[\left(1 + \frac{k_1^0}{k_D}\right)\left(\frac{Dt}{R_0^2}\right)^{1/2}\right]. \quad (15)$$

The initial value of this expression is k_1^0 while its asymptotic value is $k_1 = k_1^0 k_D/(k_1^0 + k_D)$, where $k_D = 4\pi D R_0$ is the Smoluchowski rate constant[44] for a diffusion-controlled reaction. Thus, from the fit of this formula (given in Eq. (15)) to the simulation data we can extract k_1^0 and R_0, since the value of the diffusion coefficient is known analytically for MPC dynamics.[31,32] From the data in the equation we find $k_1^0 = 11.8$ and $R_0 = 2.8$. Note that $R_0 > \sigma_C$, which accounts for the presence of a boundary layer in the vicinity of the catalytic sphere surface where the continuum diffusion equation description fails. If the C sphere were a hard sphere with radius R_0, k_1^0 has the form, $k_1^0 = p_+ R_0^2 \sqrt{8\pi k_B T/m}$. This yields the value $k_1^0 = 8.965$ for $p_+ = 1.0$.

The computation of nonequilibrium steady state concentration fields is more difficult due to the presence of noncatalytic sphere N. A crude estimate for this concentration field can be obtained by neglecting the presence of the noncatalytic sphere, so that spherical symmetry can be assumed for the solution of the reaction-diffusion equation. Figure 6 shows the effect of the presence of the N sphere on the concentration field obtained from the simulation. The presence of the N sphere leads to a reduction of $n_B(r)$ in its vicinity, which can affect the sphere dimer velocity.

In order to obtain the dimer velocity V_z from Eq. (5) one needs to specify ζ, the friction coefficient of the sphere dimer. The friction coefficient may be approximated by the sum of the friction coefficients of the two monomers $\zeta = \zeta_C + \zeta_N$. The friction coefficient of a single monomer may be estimated using $\zeta_S^{-1} = \zeta_m^{-1} + \zeta_h^{-1}$, which accounts for both microscopic, ζ_m, and hydrodynamic, ζ_h, contributions to the friction coefficient.[45] We take a simple collision model for the microscopic contribution, $\zeta_m = \frac{8}{3} n \sigma_S^2 \sqrt{2\pi m k_B T}$, and a Stokes law form for the hydrodynamic contribution, $\zeta_h = 4\pi\eta\sigma_S$, where n is the total number density of the solvent and η is the viscosity. The viscosity is known analytically for the MPC solvent.[31,32,46,47] While the friction coefficient can be determined accurately from simulations of the nanodimer subjected to an external force,[48] here for simplicity we take the value $\zeta = 80.8$, from above analytical calculation.

B. Propulsion velocities

With a knowledge of the basic parameters and assumptions that enter the theoretical calculation in hand, we turn back to the main topic of this paper, the propulsion velocity of the sphere dimer in an active medium. For the cubic autocatalytic reaction, this entails the solution of the steady state reaction-diffusion equation,

$$D\nabla^2 n_B(\mathbf{r},t) = k_2 n_B(\mathbf{r},t) n_A^2(\mathbf{r},t) - k_{-2} n_A^3(\mathbf{r},t), \tag{16}$$

subject to the boundary condition,

$$-k_1^0 n_A(R_0) + k_{-1}^0 n_B(R_0) = 4\pi D R_0^2 \frac{d}{dr} n_B(r)\Big|_{R_0}, \tag{17}$$

at the surface around the C sphere with radius R_0 and a reflecting boundary condition at the N sphere. Boundary conditions at infinity must also be specified. As $r \to \infty$ we assume that the concentration fields are given by the steady state values of the cubic autocatalytic reaction in the bulk phase: $k_2 \bar{n}_B \bar{n}_A^2 = k_{-2} \bar{n}_A^3$. In our model the spatial variations in the total density can be neglected so that $n_A(\mathbf{r},t) + n_B(\mathbf{r},t) = n_0$. Using the fact that the total density is fixed we have $\bar{n}_B = n_0(1 + k_2/k_{-2})^{-1}$ and $\bar{n}_A = n_0(1 + k_{-2}/k_2)^{-1}$.

In order to obtain analytical estimates for the solutions to the reaction-diffusion equation, two approximations are necessary. First, in a full description a reflecting boundary condition should be applied at the N sphere but, as discussed earlier, this considerably complicates the solution since the problem no longer has spherical symmetry. However, as we have seen in Fig. 6, neglect of the N sphere when computing the concentration fields has only a moderately small quantitative effect on the concentration fields of interest. Second, since the reaction-diffusion equation is nonlinear, we seek a solution that is linear in deviations from the asymptotic values of the concentration fields: $n_B(r) = \bar{n}_B + \delta n_B(r)$ and $n_A(r) = \bar{n}_A - \delta n_A(r)$. The linearized steady state reaction diffusion equation reads

$$D\nabla^2 \delta n_B(\mathbf{r},t) = (k_2 + k_{-2})\bar{n}_A^2 \delta n_B(\mathbf{r},t). \tag{18}$$

With the above boundary conditions at the catalytic sphere surface and at infinity the steady state solution is

$$n_B(r) = \bar{n}_B + \frac{\left(k_1^0 \bar{n}_A - k_{-1}^0 \bar{n}_B\right) k_D}{k_1^0 + k_{-1}^0 + k_D(1 + \kappa R_0)} \frac{e^{-\kappa(r - R_0)}}{4\pi D r}. \tag{19}$$

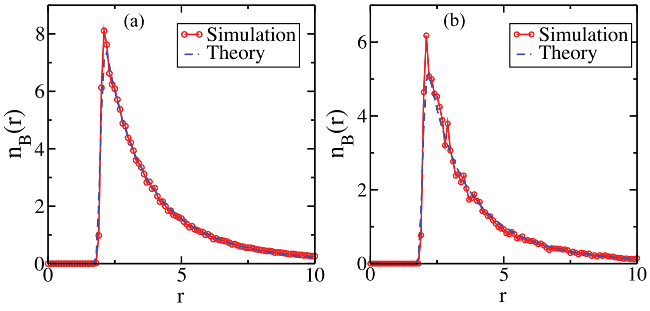

FIG. 7. Comparison of the steady state B particle concentration field $n_B(r)$ around the catalytic sphere obtained from simulation and (a) from Eq. (19) with $k_2 = 10^{-4}$ and (b) from Eq. (20) with $k_3 = 0.01$ for the irreversible reactions.

TABLE I. Average velocities of the center-of-mass of the sphere dimer along its internuclear axis. Results in the top part of the Table show the comparison of the propulsion velocity of the nanodimer obtained from the simulation (V_z^S) and reaction-diffusion theory (V_z^T) for the irreversible cubic autocatalytic reaction in the bulk phase. The bottom part of the Table shows the velocity comparison between simulation and theory for the irreversible linear reaction in the bulk phase.

k_2	0.0001	0.0002	0.0005	0.0008	0.001
V_z^T	0.056	0.050	0.040	0.035	0.033
V_z^S	0.031	0.029	0.023	0.019	0.018
k_3	0.001	0.005	0.01	0.02	0.05
V_z^T	0.053	0.043	0.036	0.029	0.02
V_z^S	0.027	0.024	0.020	0.014	0.006

Here $\kappa = \sqrt{(k_2 + k_{-2})\bar{n}_A^2/D}$ is an inverse length. The form of the A concentration field follows from the conservation condition, $n_A(r) = n_0 - n_B(r)$.

The steady state concentration field of B particles for the irreversible linear bulk phase reaction $B \to D$ with rate constant k_3 is

$$n_B(r) = \frac{k_1^0 n_0 k_D}{\left(k_1^0 + k_D\right)(1 + \kappa R_0)} \frac{e^{-\kappa(r - R_0)}}{4\pi D r}, \tag{20}$$

where $\kappa = \sqrt{k_3/D}$. Figure 7(a) compares the steady state B particle concentration field around the catalytic sphere obtained from simulation and from Eq. (19) when both reactions in the system are irreversible with $k_2 = 10^{-4}$. Figure 7(b) shows the analogous comparison of the concentration field obtained from the simulation and from Eq. (20) for $k_3 = 10^{-2}$. One sees good agreement between simulation and reaction-diffusion theory results.

Using these ingredients to compute V_z we obtain the results in Table I. As noted earlier, it is the fast conversion of B to A for large k_2 which gives rise to the enhanced decay of density field. In this case the concentration field agrees well with the theoretical expression and the discrepancy between the simulation results and theory is primarily due to the estimate of the friction coefficient. Nevertheless, the results are in qualitative agreement and correctly capture the trends in V_z with varying rate constant values.

V. TRANSLATIONAL AND ROTATIONAL DIFFUSION

An important characteristic feature of such small self-propelled objects is that their motion is stochastic due to thermal fluctuations. Hence they are expected to perform a persistent random walk, due to a competition between directed motion, with a velocity that depends on the concentration of the reactive molecules, and angular randomization due to the thermal rotational Brownian motion.[23,49–52] The transition between the two regimes depend on the rotational diffusion time τ_R of the sphere dimer. For time scales long compared to τ_R, the active particles therefore perform a random walk with a substantially enhanced diffusion coefficient given by

$$D_{\text{eff}} = D_0 + \frac{1}{3} V_z^2 \tau_R, \tag{21}$$

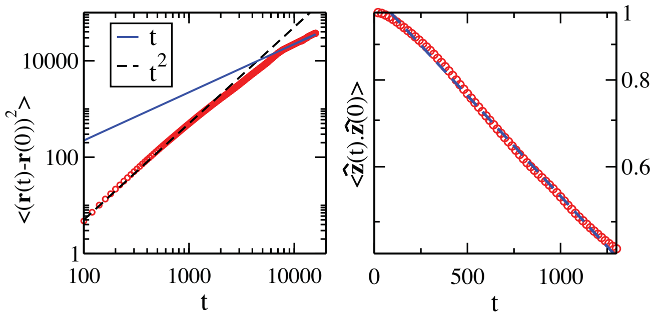

FIG. 8. (a) Log-log plot of the mean squared displacement of the nanodimer showing ballistic motion, $\Delta L^2(t) \sim t^2$, at short times and diffusive motion, $\Delta L^2(t) \sim t$, at long times for $k_2 = 0.0001$. (b) Linear-log plot of the orientational correlation function for the nanodimer as a function of time for $k_2 = 0.0001$. The dashed line is an exponential fit to the data.

where D_0 is the diffusion coefficient of the non-active particle.

We calculated the effective diffusion coefficient D_{eff} of the sphere dimer for the irreversible bulk phase cubic autocatalytic reaction by computing its mean square displacement and compared it with the result in Eq. (21). Figure 8(a) shows the mean squared displacement $\Delta L^2(t) = \langle[\mathbf{r}(t) - \mathbf{r}(0)]^2\rangle$ for the nanodimer. One can see the initial ballistic regime characterized by $\Delta L^2(t) \sim t^2$ and late time diffusive regime, where $\Delta L^2(t) = 6D_{\text{eff}}t$. The rotational diffusion time τ_R, which characterizes the orientational relaxation of the sphere dimer is defined by the decay of the orientation autocorrelation function, $\langle\hat{\mathbf{z}}(t) \cdot \hat{\mathbf{z}}(0)\rangle = e^{-t/\tau_R}$. The relaxation time τ_R was calculated by fitting an exponential to the orientation autocorrelation function as shown in Fig. 8(b). We find $\tau_R \approx 2000$ independent of propulsion velocity.

A good agreement between the enhanced diffusion coefficient D_{eff} obtained from mean square displacement calculation and that obtained from Eq. (21) is found and shown in Fig. 9.

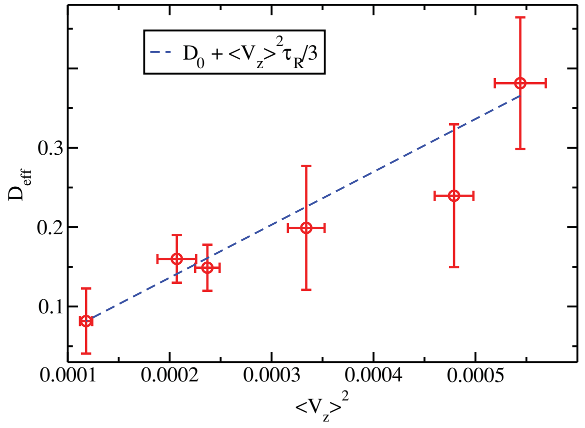

FIG. 9. Plot of the effective diffusion coefficient D_{eff} as a function of $\langle V_z\rangle^2$ for the self-propelled sphere dimer obtained from simulation (points). The average sphere dimer velocity $\langle V_z\rangle$ was determined from an average of five independent realizations of the dynamics. The dashed line is the fit from Eq. (21).

VI. CONCLUSION

Research into synthetic chemically powered motors is still at an early stage. New motors are being fabricated, the mechanisms for their motion are being understood and applications for their uses are being discovered. In almost all applications that are envisaged the motor will have to move in a complex environment that contains many, often reactive, chemical species. Any biological application will certainly be of this type. Most chemically powered motors that have been devised rely on species in their environment for fuel. If either the reactants that power the motor or products of the reaction are themselves involved in other chemical reactions in the environment, this can have a significant effect on the propulsion properties of the motor, as demonstrated in this paper. We have only considered some of the simplest ways in which a chemically active medium can influence motor motion.

In addition to being able to understand how a motor responds to chemical reactivity in the environment, one can imagine situations where reactions in the environment can be used to assist or modify motor dynamics for specific tasks. As in the cubic autocatalysis example studied in this paper, it may be possible to regenerate fuel locally where it is needed by environmental reactions that are themselves driven far from equilibrium by input of reagents at the boundaries. Since it is known that the efficiency of reaction networks is often greater when species are input in an oscillatory fashion,[53] it may be possible to improve the efficiency of synthetic motors by oscillatory reactions in the bulk phase in which they move. The fact that the motors rely for their propulsion on nonequilibrium conditions sets the stage for other far-from-equilibrium chemical phenomena in the environment. We have demonstrated that sphere dimer motors can be reflected by chemical waves,[54] possibly providing a mechanism for the control of their motion. Systems in nature display variety of stationary and dynamical chemical patterns with a wide range of length and time scales.[55] Chemically powered motors may be able to exploit the patterns in these systems to move in specific ways in the system to perform their tasks. The work presented in this paper provides an introduction to some of the phenomena to be expected for chemically powered motors in chemically active media.

ACKNOWLEDGMENTS

Research supported in part by a grant from the Natural Sciences and Engineering Research Council of Canada. Computations were performed on the GPC supercomputer at the SciNet HPC Consortium. SciNet is funded by: the Canada Foundation for Innovation under the auspices of Compute Canada; the Government of Ontario; Ontario Research Fund - Research Excellence; and the University of Toronto.

[1] R. D. Vale and R. A. Milligan, Science **288**, 88 (2000).
[2] J. E. Molloy and C. Veigel, Science **300**, 2045 (2003).
[3] W. F. Paxton, K. C. Kistler, C. C. Olmeda, A. Sen, S. K. St. Angelo, Y. Cao, T. E. Mallouk, P. E. Lammert, and V. H. Crespi, J. Am. Chem. Soc. **126**, 13424 (2004).
[4] T. R. Kline, W. F. Paxton, T. E. Mallouk, and A. Sen, Angew. Chem., Int. Ed. **44**, 744 (2005).

[5] W. F. Paxton, S. Sundararajan, T. E. Mallouk, and A. Sen, Angew. Chem., Int. Ed. **45**, 5420 (2006).

[6] S. Fournier-Bidoz, A. C. Arsenault, I. Manners, and G. A. Ozin, Chem. Commun. (Cambridge), **2005**, 441.

[7] G. A. Ozin, I. Manners, S. Fournier-Bidoz, and A. Arsenault, Adv. Mater. **17**, 3011 (2005).

[8] Y. Wang, R. M. Hernandez, D. J. Bartlett, Jr., J. M. Bingham, T. R. Kline, A. Sen, and T. E. Mallouk, Langmuir **22**, 10451 (2006).

[9] R. Laocharoensuk, J. Burdick, and Y. Wang, ACS Nano **5**, 1069 (2008).

[10] W. F. Paxton, A. Sen, and T. E. Mallouk, Angew. Chem., Int. Ed. **11**, 6462 (2005).

[11] J. Burdick, R. Laocharoensuk, P. M. Wheat, J. D. Posner, and J. Wang, J. Am. Chem. Soc. **130**, 8164 (2008).

[12] A. Ghosh and P. Fischer, Nano Lett. **9**, 2243 (2009).

[13] N. Mano and A. Heller, J. Am. Chem. Soc. **127**, 11574 (2005).

[14] D. Kagan, P. Calvo-Marzal, S. Balasubramanian, S. Sattayasamitsathit, K. M. Manesh, G. Flechsig, and J. Wang, J. Am. Chem. Soc. **131**, 12082 (2009).

[15] L. F. Valadares, Y. Tao, N. S. Zacharia, V. Kitaev, F. Galembeck, R. Kapral, and G. A. Ozin, Small **6**, 565 (2010).

[16] H. Ke, S. Ye, R. L. Carroll, and K. Showalter, J. Phys. Chem. A **114**, 5462 (2010).

[17] G. Rückner and R. Kapral, Phys. Rev. Lett. **98**, 150603 (2007).

[18] Y.-G. Tao and R. Kapral, J. Chem. Phys. **128**, 164518 (2008).

[19] S. Thakur and R. Kapral, J. Chem. Phys. **133**, 204505 (2010).

[20] R. Golestanian, T. B. Liverpool, and A. Ajdari, Phys. Rev. Lett. **94**, 220801 (2005).

[21] R. Golestanian, T. B. Liverpool, and A. Ajdari, New J. Phys. **9**, 126 (2007).

[22] A. Erbe, M. Zientara, L. Baraban, C. Kreidler, and P. Leiderer, J. Phys. Condens. Matter **20**, 404215 (2008).

[23] J. R. Howse, R. A. L. Jones, A. J. Ryan, T. Gough, R. Vafabakhsh, and R. Golestanian, Phys. Rev. Lett. **99**, 048102 (2007).

[24] S. Ebbens, R. A. L. Jones, A. J. Ryan, R. Golestanian, and J. R. Howse, Phys. Rev. E **82**, 015304 (2010).

[25] M. N. Popescu, S. Dietrich, M. Tasinkevych, and J. Ralston, Eur. Phys. J. E **31**, 351 (2010).

[26] A. Malevanets and R. Kapral, J. Chem. Phys. **110**, 8605 (1999).

[27] A. Malevanets and R. Kapral, J. Chem. Phys. **112**, 72609 (2000).

[28] K. Rohlf, S. Fraser, and R. Kapral, Comput. Phys. Commun. **179**, 132 (2008).

[29] K. Tucci and R. Kapral, J. Phys. Chem. B **109**, 21300 (2005).

[30] C. Echeverria and R. Kapral, Physica D **239**, 791 (2010).

[31] R. Kapral, Adv. Chem. Phys. **140**, 89 (2008).

[32] G. Gompper, T. Ihle, D. M. Kroll, and R. G. Winkler, Adv. Polym. Sci. **221**, 1 (2009).

[33] F. C. Collins and G. E. Kimball, J. Colloid Sci. **4**, 425 (1949).

[34] D. Frenkel and B. Smit, *Understanding Molecular Simulation - From Algorithms to Applications* (Academic, San Diego, 1996).

[35] H. C. Andersen, J. Comput. Phys. **52**, 24 (1983).

[36] T. Ihle and D. M. Kroll, Phys. Rev. E **63**, 020201 (2001).

[37] T. Ihle and D. M. Kroll, Phys. Rev. E **67**, 066705 (2003).

[38] This is the case for the iodate-arsenous acid reaction whose overall kinetics is accurately described by cubic autocatalysis. However, the actual mechanism is quite complex and the overall rate equation is obtained by eliminating fast intermediate species from the rate equations. See A. Saul and K. S. Showalter, in *Oscillations and Traveling Waves in Chemical Systems*, edited by R. J. Field and M. Burger (Wiley-Interscience, New York, 1985), pp. 419–439.

[39] S. R. de Groot and P. Mazur, *Nonequilibrium Thermodynamics* (North-Holland, Amsterdam, 1962).

[40] It is well known that detailed balance must be broken for directed motion and this feature enters in models for ratchets and molecular motors. See, for example, R. D. Astumian, Science **276**, 917 (1997); P. Reimann, Phys. Rep. **361**, 57 (2002).

[41] A similar calculation was carried out for a hard sphere model for the catalytic reaction in Ref. 43. Our particles interact with the catalytic sphere by repulsive LJ potentials and the simulations reported here provide accurate estimates of the parameters needed for the theoretical model. Applications of similar methods to enzyme kinetics are given in J.-X. Chen and R. Kapral, J. Chem. Phys. **134**, 044503 (2011).

[42] R. Kapral, Adv. Chem. Phys. **48**, 71 (1981).

[43] K. Tucci and R. Kapral, J. Chem. Phys. **120**, 8262 (2004).

[44] M. von Smoluchowski, Ann. Phys. **48**, 1003 (1915).

[45] S. H. Lee and R. Kapral, J. Chem. Phys. **121**, 11163 (2004).

[46] M. Ripoll, K. Mussawisade, R. G. Winkler, and G. Gompper, Phys. Rev. E **72**, 016701 (2005).

[47] N. Kikuchi, C. M. Pooley, J. F. Ryder, and J. M. Yeomans, J. Chem. Phys. **119**, 6388 (2003).

[48] Y.-G. Tao and R. Kapral, J. Chem. Phys. **131**, 024113 (2009).

[49] R. Golestanian, Phys. Rev. Lett. **102**, 188305 (2009).

[50] H. C. Berg, *E. coli in Motion* (Springer-Verlag, New York, 2004).

[51] J. Palacci, C. Cottin-Bizonne, C. Ybert, and L. Bocquet, Phys. Rev. Lett. **105**, 088304 (2010).

[52] F. Peruani and L. G. Morelli, Phys. Rev. Lett. **99**, 010602 (2007).

[53] Y. Termonia and J. Ross, Proc. Natl. Acad. Sci. U.S.A. **78**, 2952 (1981).

[54] S. Thakur and R. Kapral, Angew. Chem., Int. Ed. (in press).

[55] R. C. Desai and R. Kapral, *Dynamics of Self-Organized and Self-Assembled Structures* (Cambridge University Press, Cambridge, England, 2009).

[56] Similar considerations apply to the quadratic autocatalytic reaction, $B + A \rightleftharpoons 2A$. Cubic autocatalysis was chosen in this study since, in applications where the active medium exhibits a chemical front where A consumes B, cubic fronts have a simpler structure than quadratic fronts [R. A. Fisher, Ann. Eugenics **7**, 335 (1937); A. Kolmogorov, I. Petrovsky, and N. Piskunov, Bull. Univ. Moscow Ser. Int. Sec. A **1**, 1 (1937); J. D. Murray, *Mathematical Biology* (Springer, Berlin, 1989)].